Supporting Information for:

Slow Magnetization Dynamics in a Series of Two-Coordinate Iron(II) Complexes

Joseph M. Zadrozny,[a] Mihail Atanasov,*[b,c,d] Aimee M. Bryan,[e] Chun-Yi Lin,[e] Brian D. Rekken,[e] Philip P. Power,*[e] Frank Neese,*[d] and Jeffrey R. Long*[a]

[a]*Department of Chemistry, University of California, Berkeley, California 94720, USA. Email: jrlong@berkeley.edub*
[b]*Max-Planck Institute for Bioinorganic Chemistry, Stifstr. 32-34, D-45470 Mülheim an der Ruhr, Germany*
[c]*Institute of General and Inorganic Chemistry, Bulgarian Academy of Sciences, Acad. Giorgi Bontchev Str. 11, 113 Sofia, Bulgaria*
[d]*Departement de Chimie, Universite de Fribourg, Ch. du Musee, 9, CH-1700 Fribourg, Switzerland, 5*
[e]*Department of Chemistry, University of California, Davis, California, 95616, USA*

Chem. Sci.

Table of Contents

Derivation of the superimposability index, R_σ.

Originally, we had planned to evaluate this index based on deviations from the Brillouin function. We tried, using $S = {}^1/_2$ and variable g for each data set, but in all cases the Brillouin function did not adequately represent a master function with which we could compare superimposability. Instead we used eq (S1) as a fitting equation, which would be weighted to fit the three highest-T data of the 1 T data set and the three lowest-T data of the 7 T set. The values of c_1, c_2, c_3, c_4, and the exponent n, determined from these fits, are given in Table 2.

$$M = \left(\frac{c_1 \left(\frac{H}{T}\right)^n}{c_2 \left(\frac{H}{T}\right)^n + c_3 \left(\frac{H}{T}\right)} \right) + c_4 \qquad \text{(S1)}$$

The experimental magnetizations were compared with these ideal, master functions, and the superimposability index, R_σ, was then defined according to eq (S2). The master functions for each complex are plotted as black lines in Figs. S1 – S6.

$$R_\sigma = \sum_i \frac{(M_{\exp,i} - M_{calc,i})^2}{M_{\exp,i}} \qquad \text{(S2)}$$

Fitted coefficients and exponents for derivation of R_σ, the superimposability index.

Complex	c_1	c_2	c_3	c_4	n	R_σ
1	1.492	0.748	0.081	1.08	3.34	0.029
2	1.487	0.658	0.075	1.01	3.13	0.027
3	2.048	1.018	0.112	0.75	3.08	0.013
4	4.969	3.428	0.494	0.73	3.16	0.062
5	6.094	3.734	0.395	0.44	2.93	0.005
6	5.788	4.354	0.865	0.62	3.38	0.135

Table S1. Crystallographic Data[a] for **1**.

Empirical formula	$C_{50}H_{52}FeN_2Si_2$
Formula weight	552.77
T, K	95(1)
λ, Å	0.7107
Crystal system	Triclinic
Space group	P–1
Habit	Block
Color	Brown
a, Å	8.8101(5)
b, Å	9.1759(5)
c, Å	11.1624(6)
α, °	102.4670(10)
β, °	92.5030(10)
γ, °	113.9320(10)
V, $Å^3$	796.59(8)
Z	1
ρ_{calc}, g/cm^3	1.152
μ, mm^{-1}	0.568
F_{000}	300
Crystal dimensions	0.368 × 0.367 × 0.358 mm^3
2θ range, °	3.78 – 55.02
Index ranges	-10 <= h <= 11
	-11 <= k <= 11
	-14 <= l <= 14
Reflections collected	8827
Independent reflections	3654 [R_{int} = 0.0140]
Completeness to 2θ = 55.02	99.6 %
Data / restraints / parameters	3654 / 167 / 0
Goodness-of-fit on F^2	1.002
Final R indices [I > 2σ(I)][b]	R_1 = 0.0345, wR_2 = 0.1035
R indices (all data)	R_1 = 0.0376, wR_2 = 0.1065
Largest diff. peak and hole	0.484 and -0.535 $eÅ^3$

[a]Obtained with graphite-monochromated Mo Kα (λ = 0.7107 Å) radiation. [b]$R_1 = \Sigma||F_o||F_c||/|F_o|$, $wR_2 = \{\Sigma[w(F_o^2 - F_c^2)^2]/\Sigma[w(F_o^2)^2]\}^{1/2}$.

Table S2. Crystallographic Data[a] for **3**.

Empirical formula	$C_{60}H_{76}Fe_{0.93}N_2$[c]
Formula weight	877.17
T, K	90(2)
λ, Å	0.7107
Crystal system	Monoclinic
Space group	$P2_1/n$
Habit	Block
Color	Red-orange
a, Å	10.8937(18)
b, Å	20.234(3)
c, Å	11.2231(19)
α, °	90
β, °	90.829(3)
γ, °	90
V, Å^3	2473.5(7)
Z	2
ρ_{calc}, g/cm^3	1.178
μ, mm^{-1}	0.325
F_{000}	948
Crystal dimensions	0.25 × 0.17 × 0.14 mm^3
2θ range, °	4.02 – 50.70
Index ranges	-13 <= h <= 13
	-24 <= k <= 24
	-13 < =l < =13
Reflections collected	27437
Independent reflections	4534 [R_{int} = 0.0416]
Completeness to 2θ = 50.70	100.0 %
Data / restraints / parameters	4534 / 0 / 298
Goodness-of-fit on F^2	1.031
Final R indices [I > 2σ(I)][b]	R_1 = 0.0338, wR_2 = 0.0800
R indices (all data)	R_1 = 0.0449, wR_2 = 0.0857
Largest diff. peak and hole	0.359 and -0.212 eÅ^3

[a]Obtained with graphite-monochromated Mo Kα (λ = 0.7107 Å) radiation. [b]$R_1 = \Sigma||F_o||F_c||/|F_o|$, $wR_2 = \{\Sigma[w(F_o^2 - F_c^2)^2]/\Sigma[w(F_o^2)^2]\}^{1/2}$. [c]Substitutional disorder between the complex and free ligand is observed, leading to a model with incomplete Fe-occupancy.

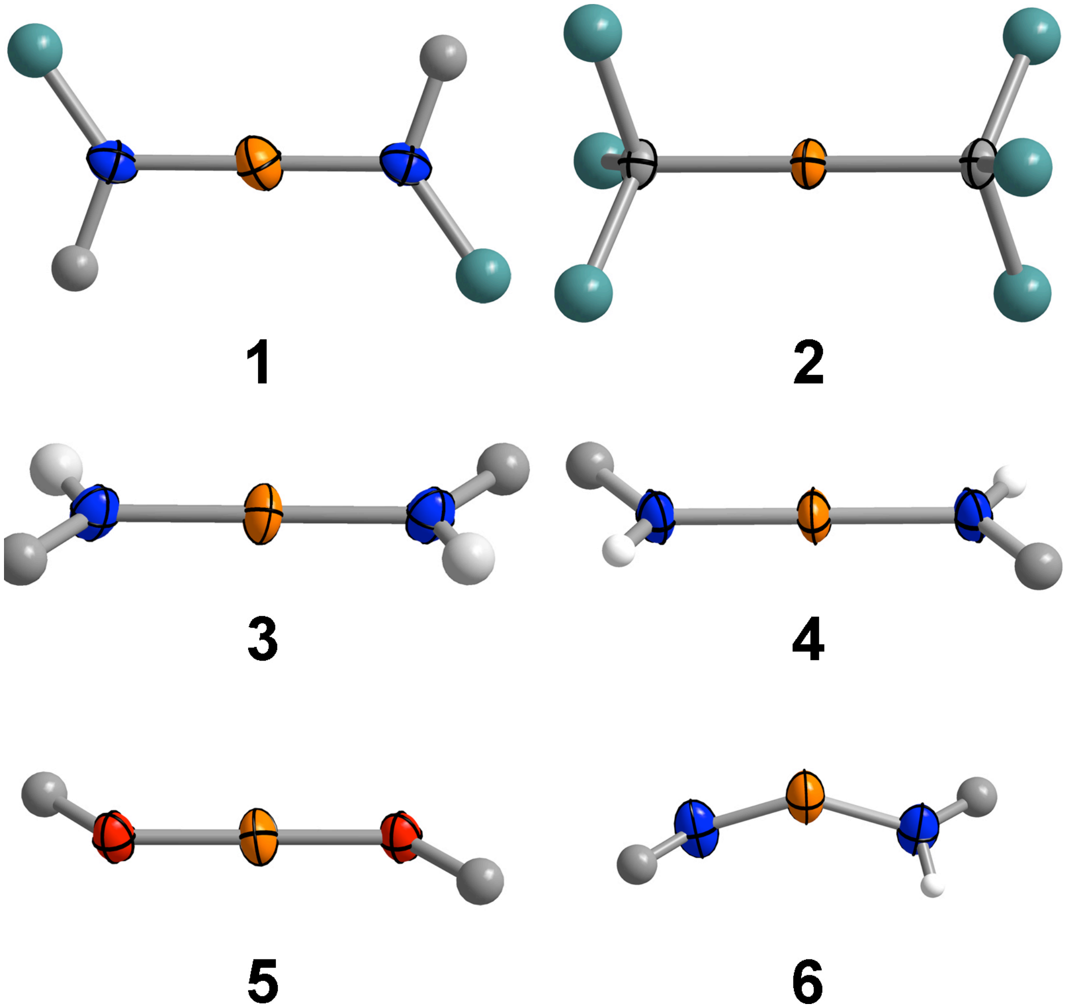

Figure S1. Probability ellipsoids of the L-Fe-L moieties for complexes **1-6,** depicted at the 80% level. Only the thermal parameters of the Fe ions and their immediate neighbors are depicted. Orange, blue, red, and gray ellipsoids correspond to Fe, N, O, and C atoms, respectively. Cyan, gray, and white spheres correspond to Si, C, and H atoms, respectively. Next-nearest structure around the donor atoms is given to assist in comparison of the principal axes of the ellipsoids with the overall molecular geometry.

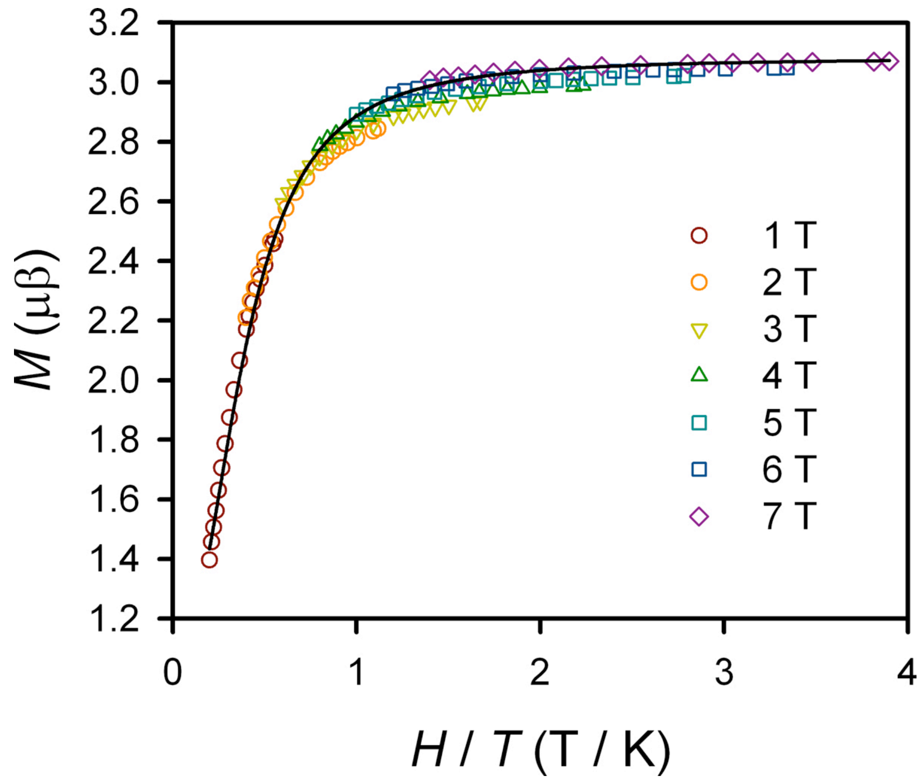

Figure S2. Variable field, variable temperature magnetization data collected on **1** from 1 to 7 T at temperatures from 1.8 to 5 K. The black line represents the master equation used to determine the superimposability index, as discussed in the main text and above.

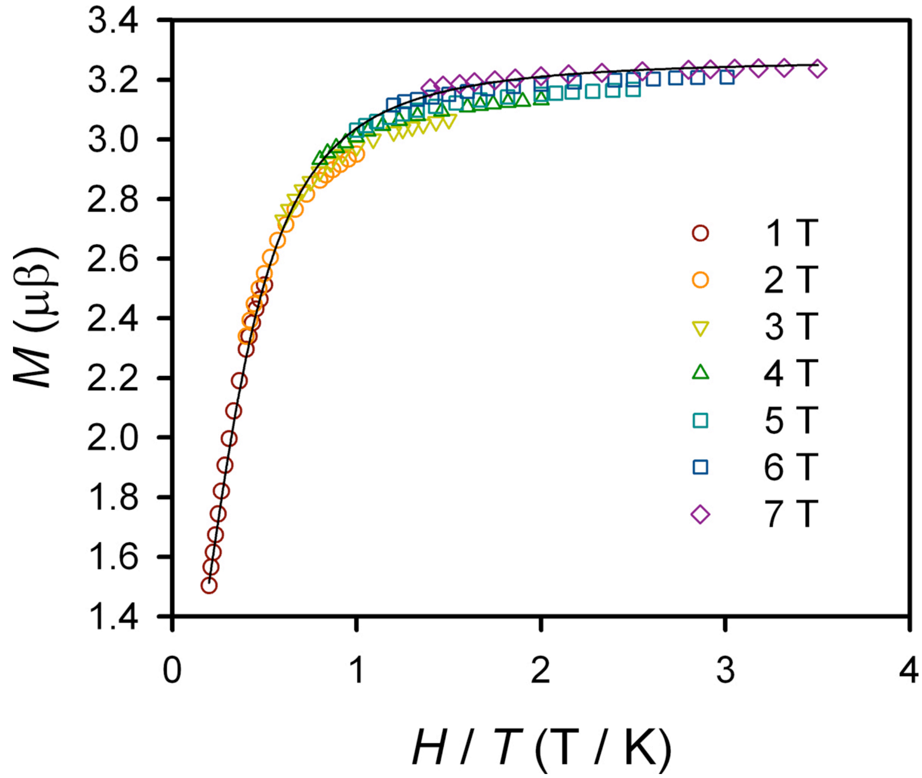

Figure S3. Variable field, variable temperature magnetization data collected on **2** from 1 to 7 T at temperatures from 1.8 to 5 K. The black line represents the master equation used to determine the superimposability index, as discussed in the main text and above.

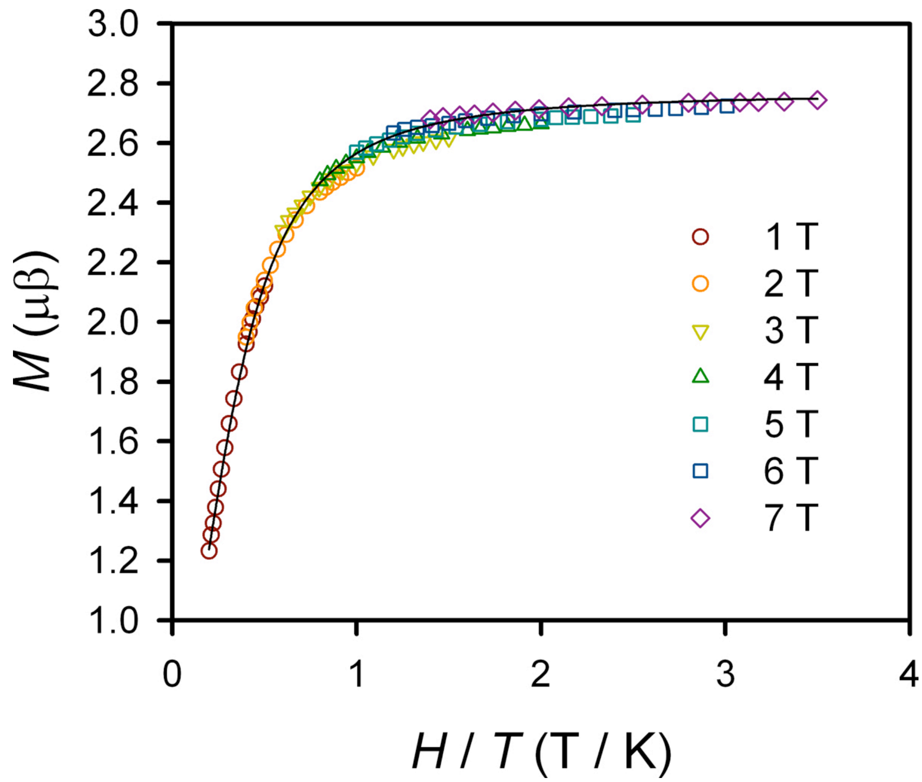

Figure S4. Variable field, variable temperature magnetization data collected on **3** from 1 to 7 T at temperatures from 1.8 to 5 K. The black line represents the master equation used to determine the superimposability index, as discussed in the main text and above.

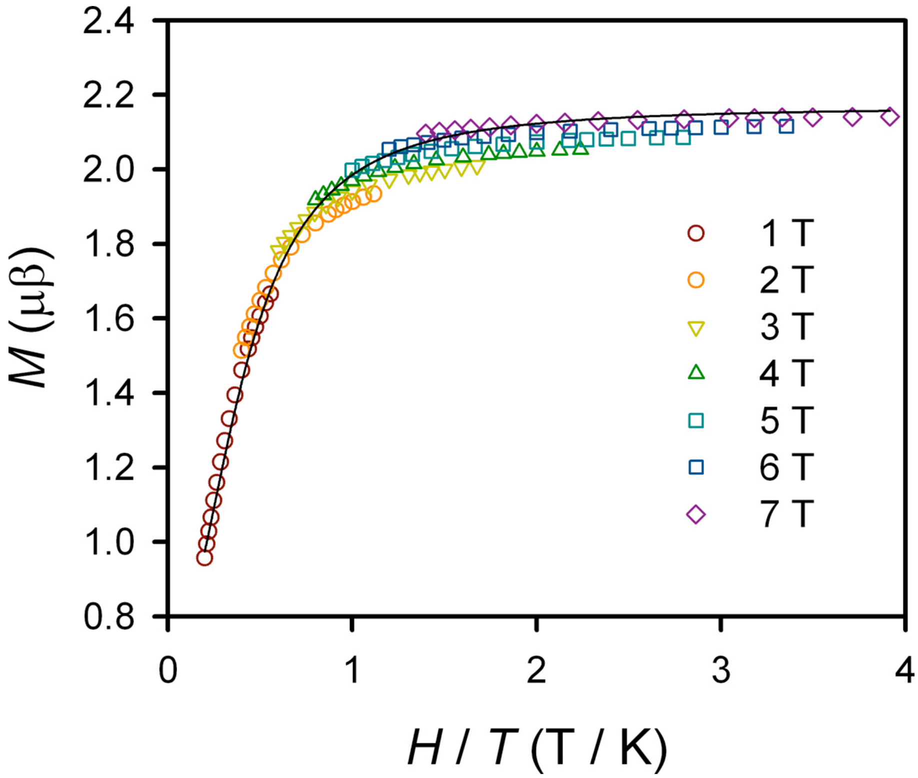

Figure S5. Variable field, variable temperature magnetization data collected on **4** from 1 to 7 T at temperatures from 1.8 to 5 K. The black line represents the master equation used to determine the superimposability index, as discussed in the main text and above.

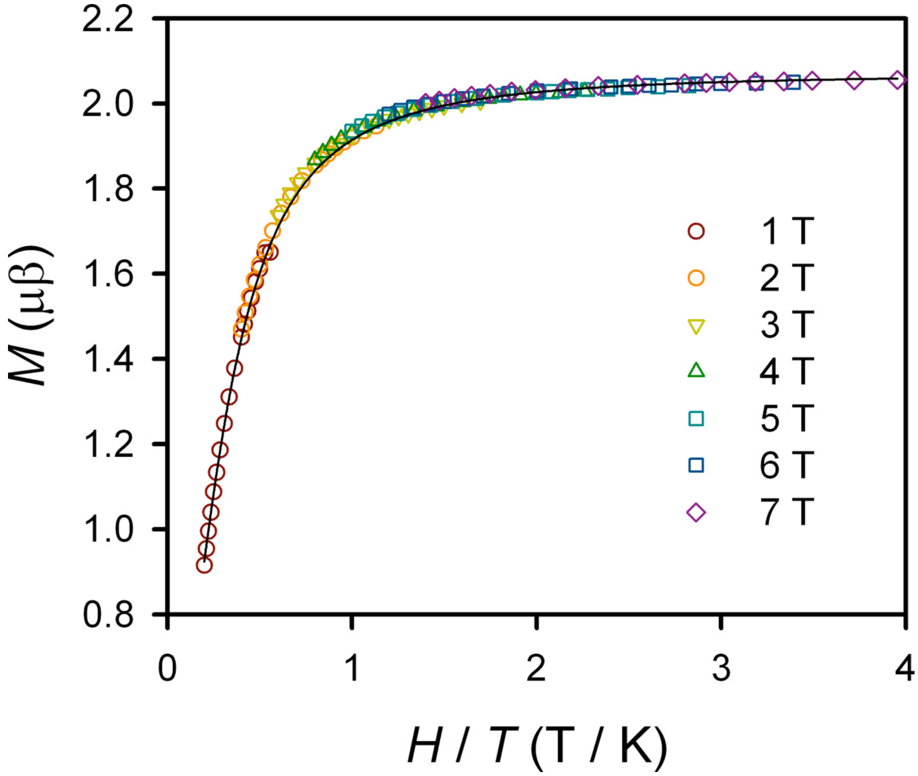

Figure S6. Variable field, variable temperature magnetization data collected on **5** from 1 to 7 T at temperatures from 1.8 to 5 K. The black line represents the master equation used to determine the superimposability index, as discussed in the main text and above.

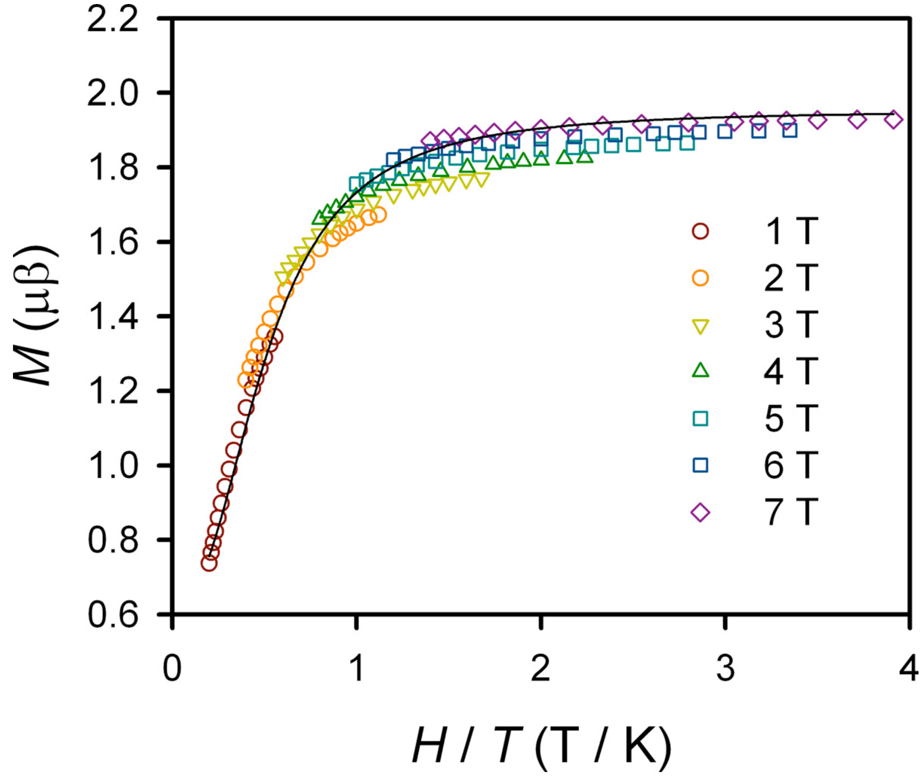

Figure S7. Variable field, variable temperature magnetization data collected on **6** from 1 to 7 T at temperatures from 1.8 to 5 K. The black line represents the master equation used to determine the superimposability index, as discussed in the main text and above.

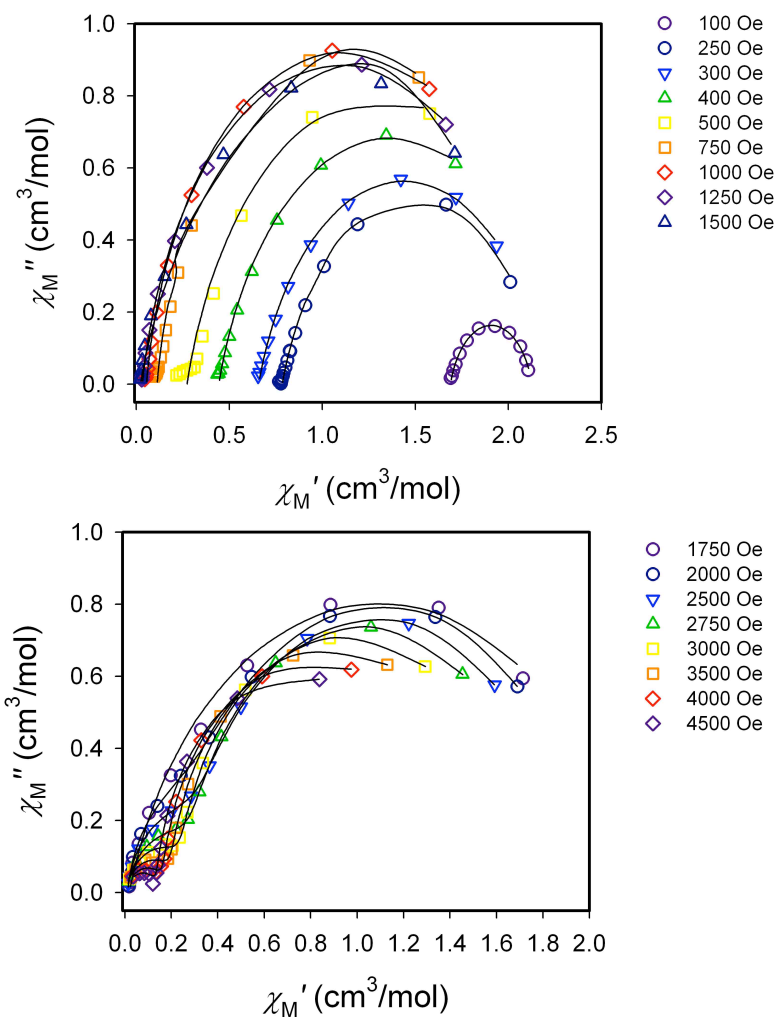

Figure S8. Cole-cole plots fit for the determination of the field dependence of τ for **1** at 2 K. Black lines are the result of fits to a generalized Debye model as described in the main text.

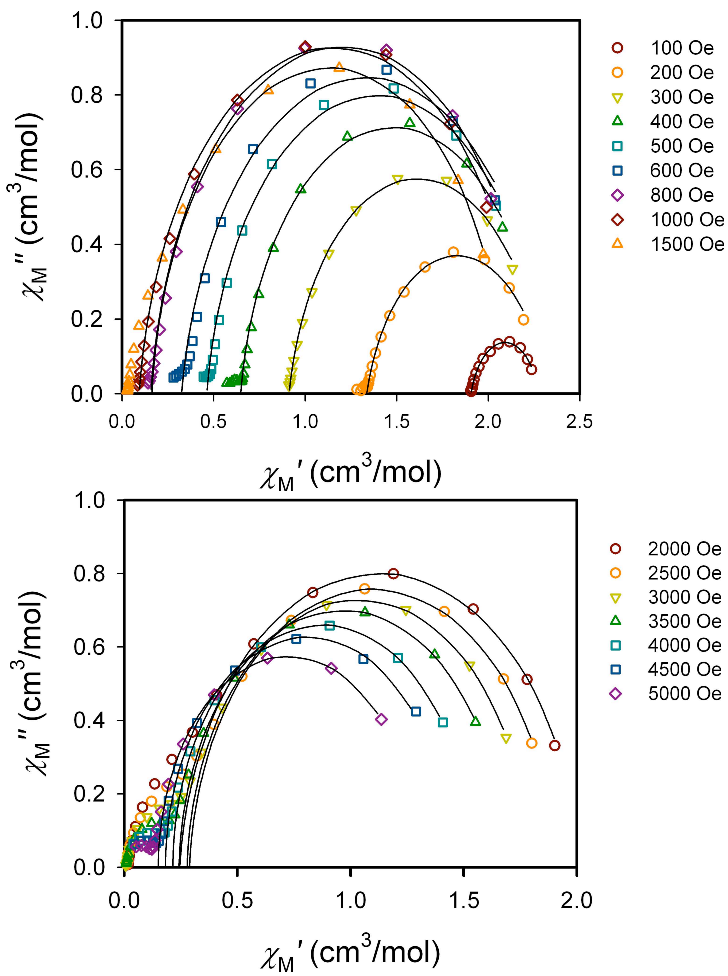

Figure S9. Cole-cole plots fit for the determination of the field dependence of τ for **2** at 2 K. Black lines are the result of fits to a generalized Debye model as described in the main text.

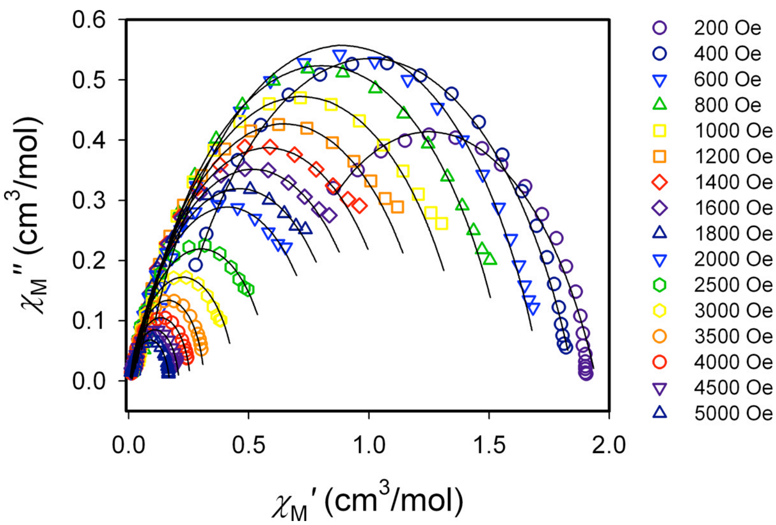

Figure S10. Cole-cole plots fit for the determination of the field dependence of τ for **3** at 2 K. Black lines are the result of fits to a generalized Debye model as described in the main text.

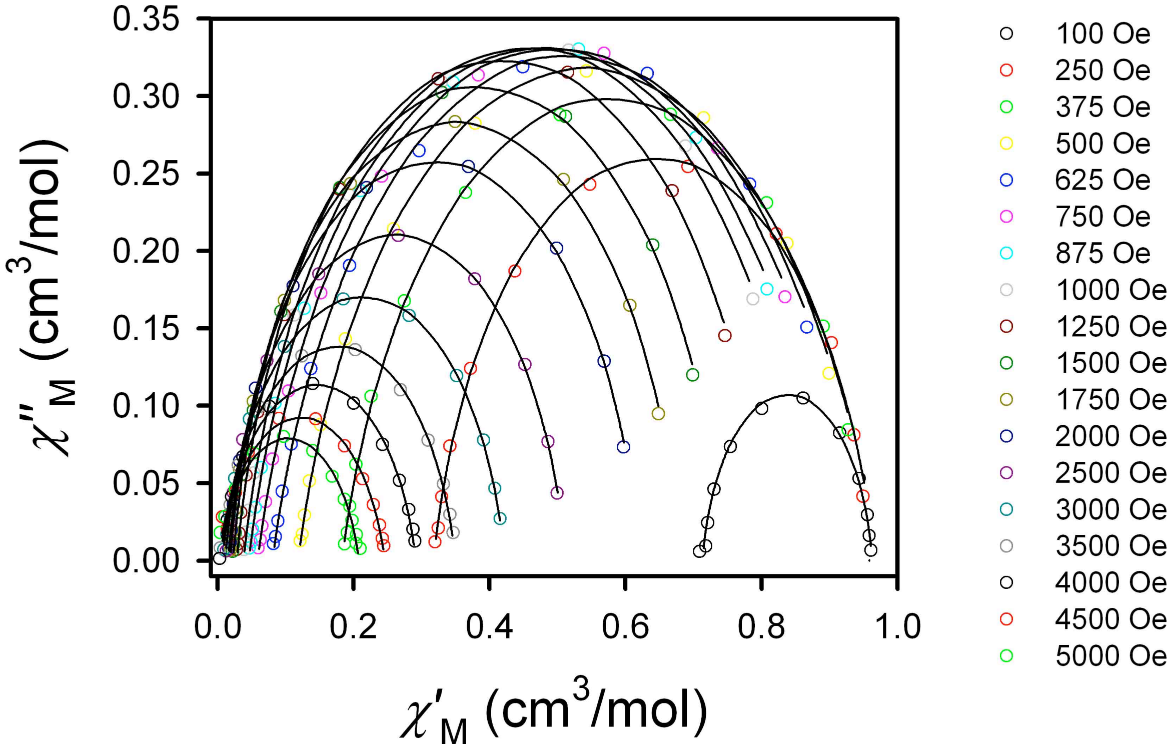

Figure S11. Cole-cole plots fit for the determination of the field dependence of τ for **4** at 2 K. Black lines are the result of fits to a generalized Debye model as described in the main text.

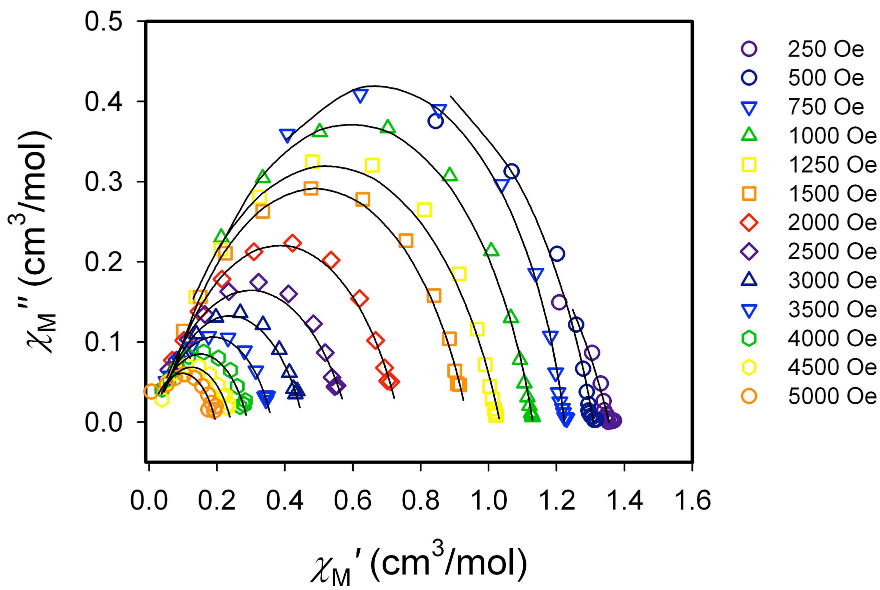

Figure S12. Cole-cole plots fit for the determination of the field dependence of τ for **5** at 2 K. Black lines are the result of fits to a generalized Debye model as described in the main text.

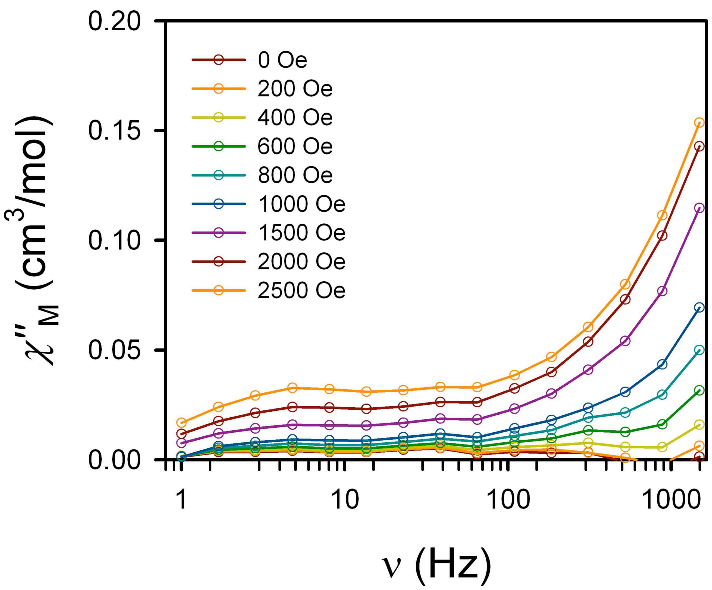

Figure S13. Frequency dependence of the out-of-phase susceptibility of **6** as a function of applied field at 2K. Solid lines are a guide for the eye.

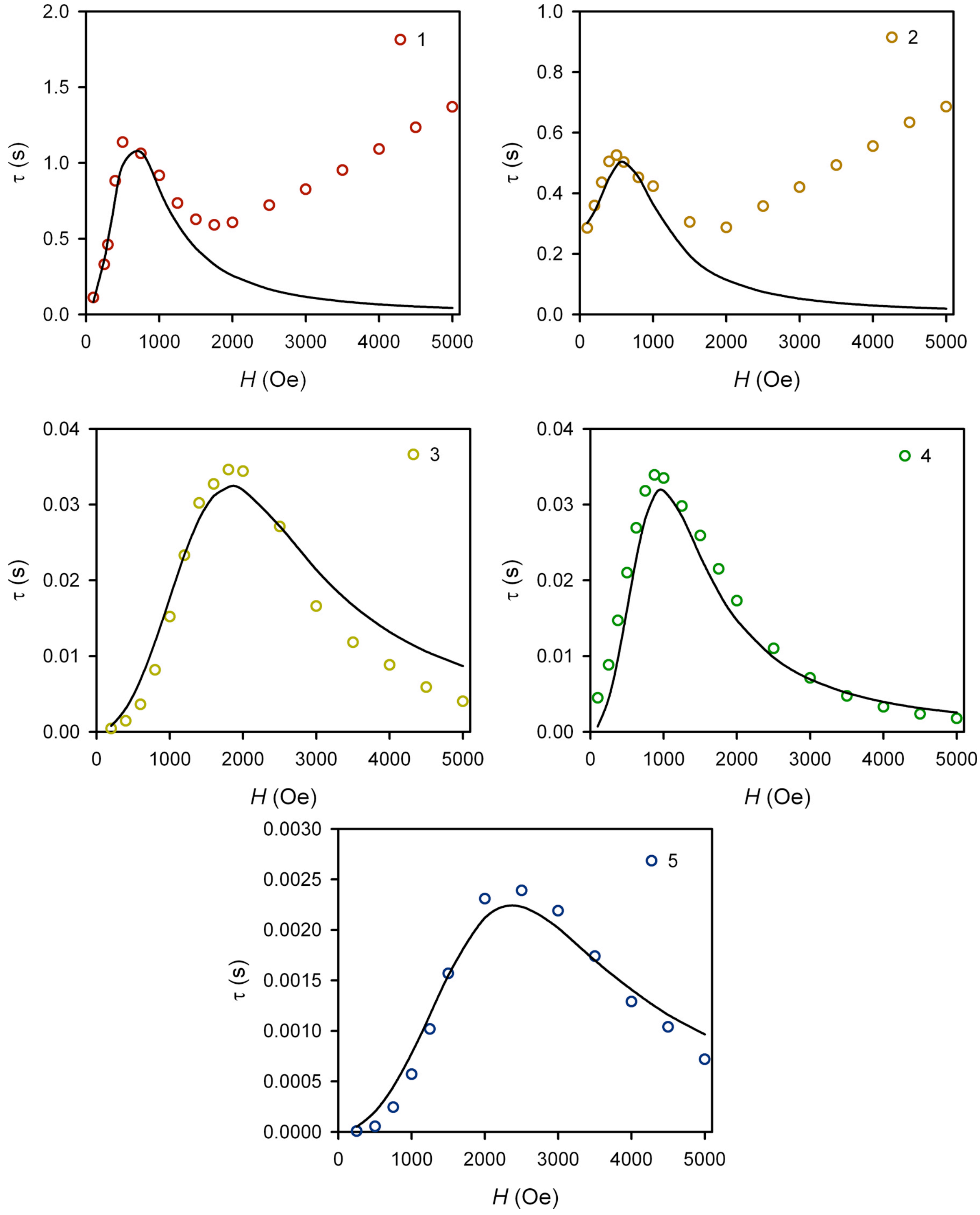

Figure S14. Field dependence of τ for **1-5** at 2 K. Black lines represent fits as discussed in the main body of the report.

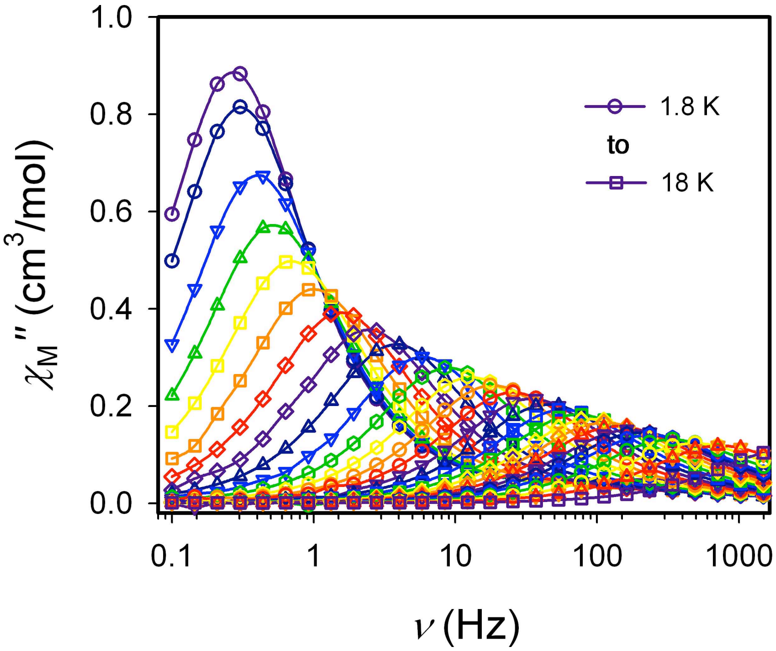

Figure S15. Frequency dependence of the out-of-phase susceptibility of **2** as a function of temperature. Data were collected under an applied dc field of 500 Oe.

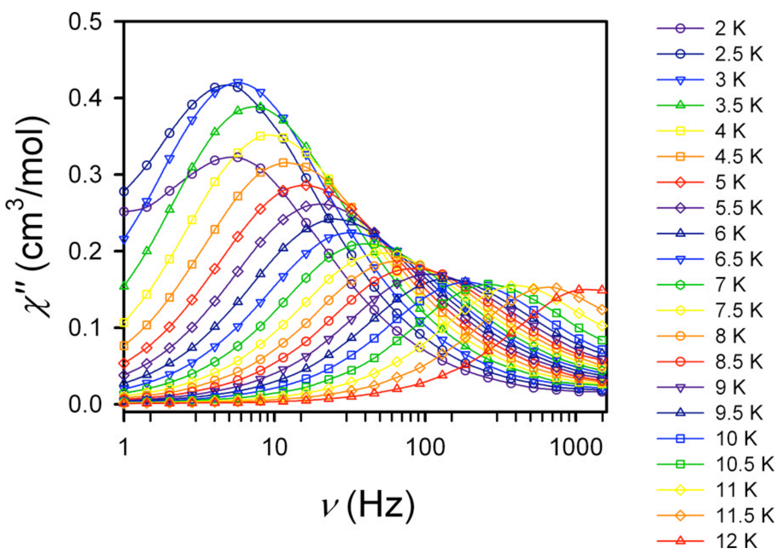

Figure S16. Frequency dependence of the out-of-phase susceptibility of **3** as a function of temperature. Data were collected under an applied dc field of 875 Oe.

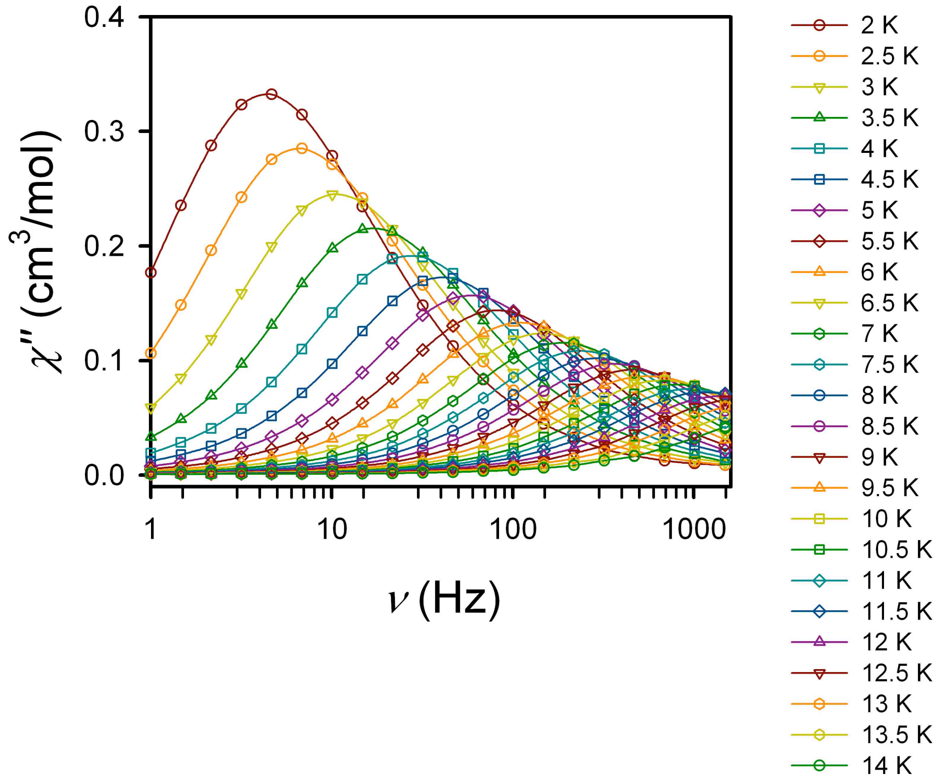

Figure S17. Frequency dependence of the out-of-phase susceptibility of **4** as a function of temperature. Data were collected under an applied dc field of 875 Oe.

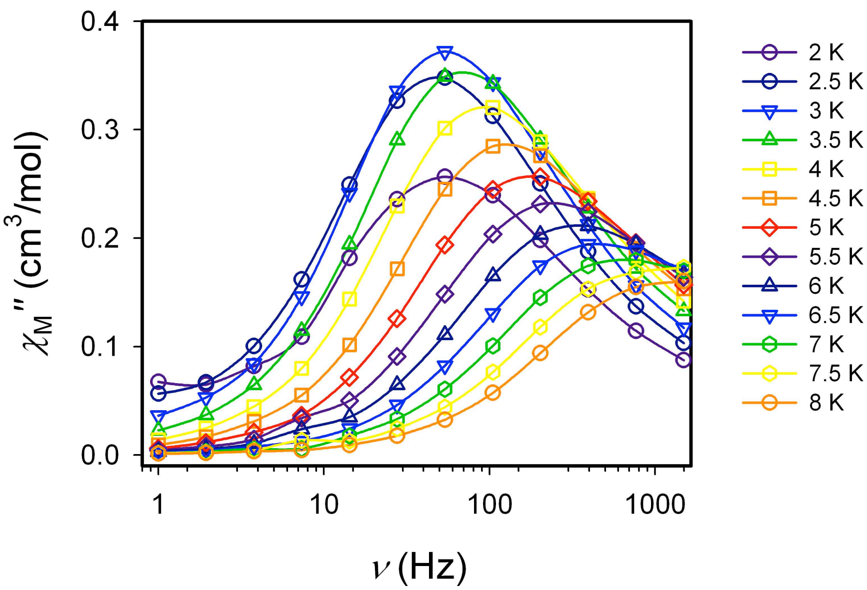

Figure S18. Frequency dependence of the out-of-phase susceptibility of **5** as a function of temperature. Data were collected under an applied dc field of 2500 Oe.

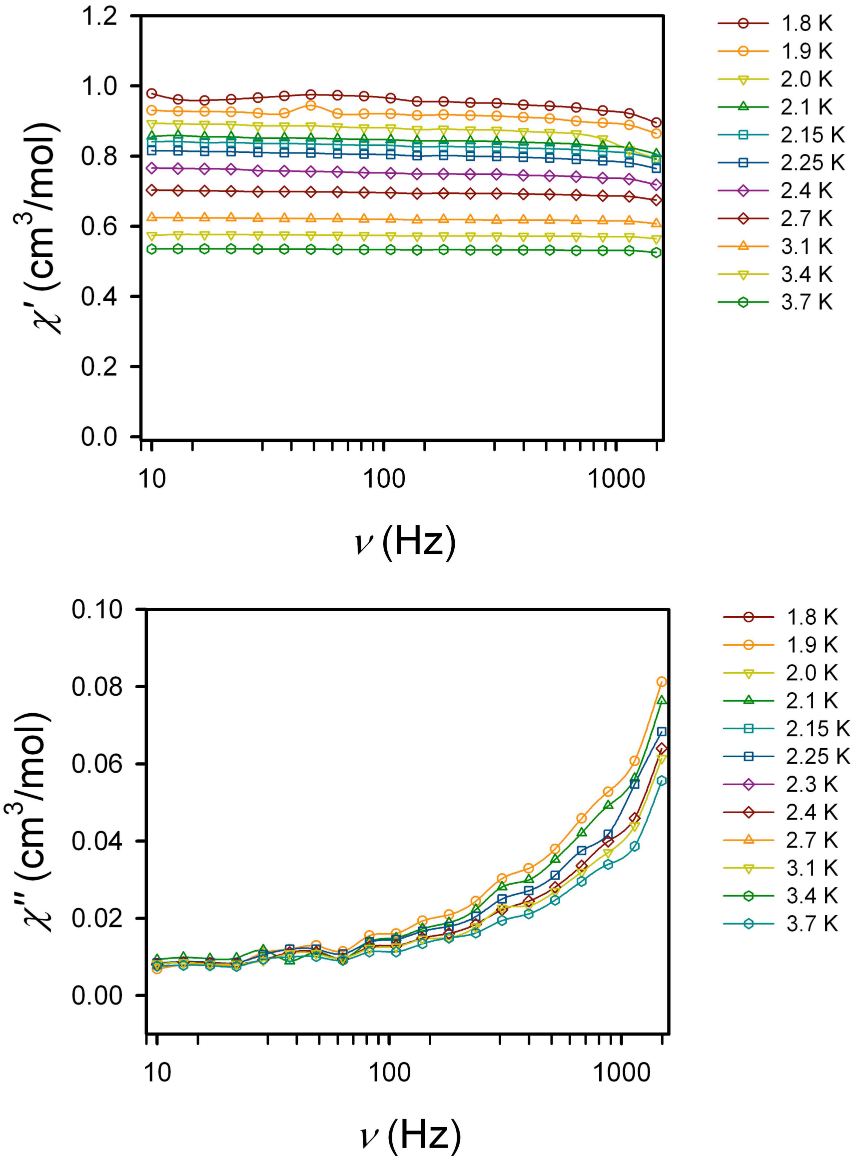

Figure S19. Frequency dependence of the in-phase (top) and out-of-phase (bottom) susceptibilities of **6** as a function of temperature. Data were collected under an applied dc field of 1000 Oe.

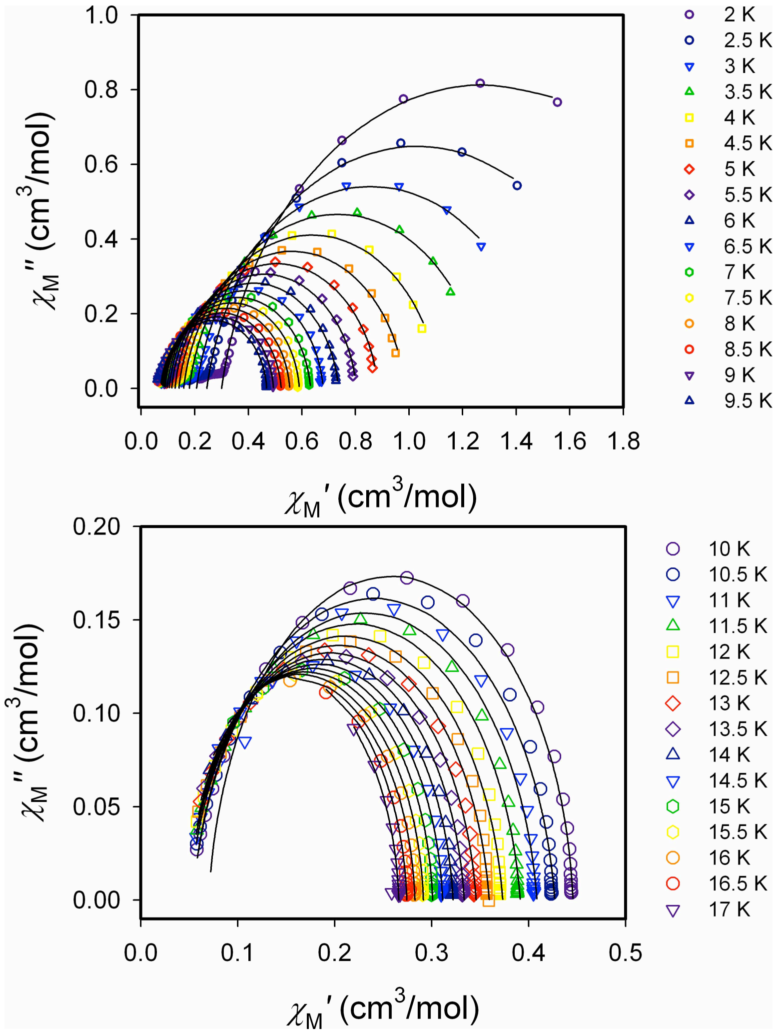

Figure S20. Cole-cole plots of the frequency dependence of χ_M' and χ_M'' used to evaluate the temperature dependence of τ for **1**. Top: data collected from 2 to 9.5 K. Bottom: data collected from 10 to 17 K. Black lines are fits to the general Debye model as described in the main text.

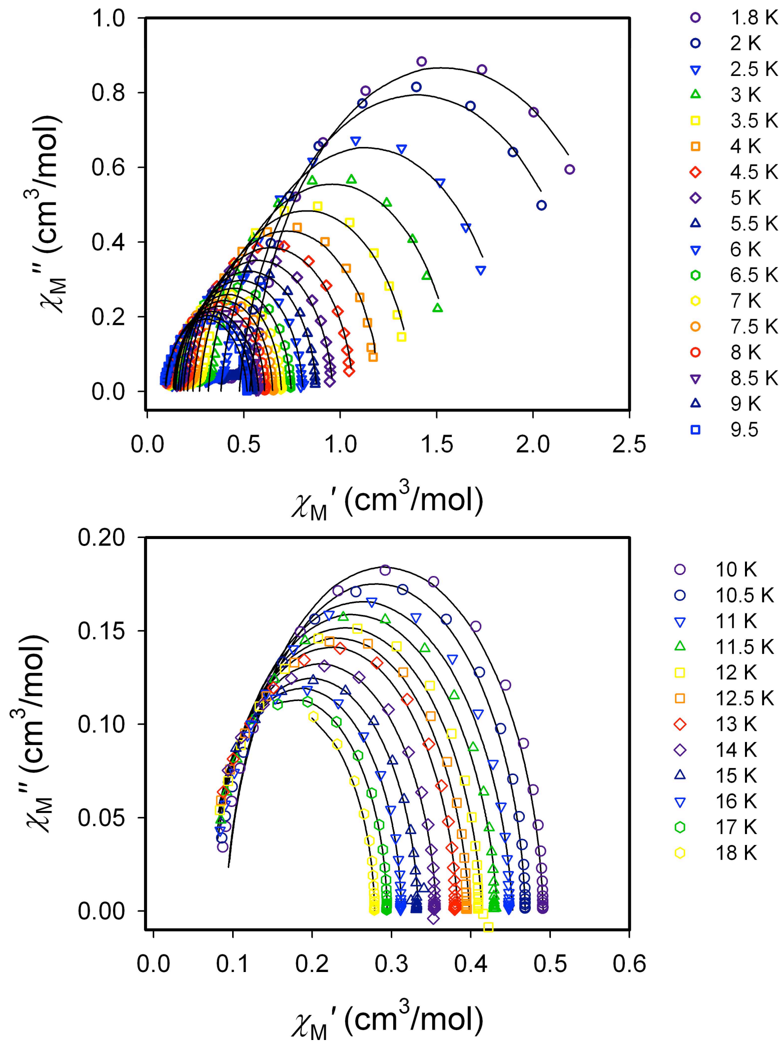

Figure S21. Cole-cole plots of the frequency dependence of χ_M' and χ_M'' used to evaluate the temperature dependence of τ for **2**. Black lines are fits to the general Debye model as described in the main text.

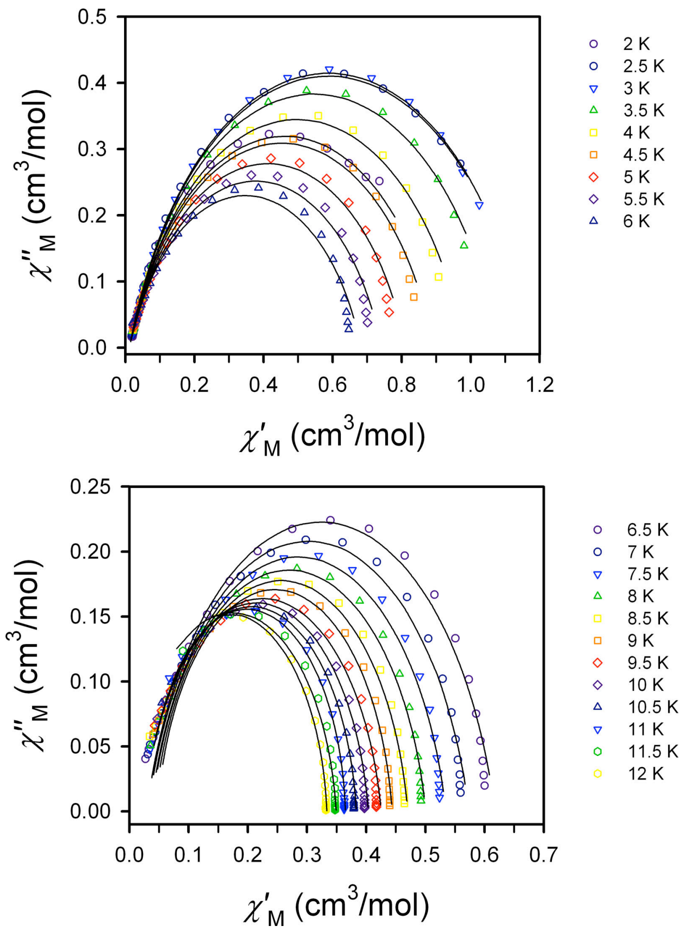

Figure S22. Cole-cole plots of the frequency dependence of χ_M' and χ_M'' used to evaluate the temperature dependence of τ for **3**. Black lines are fits to the general debye model as described in the main text.

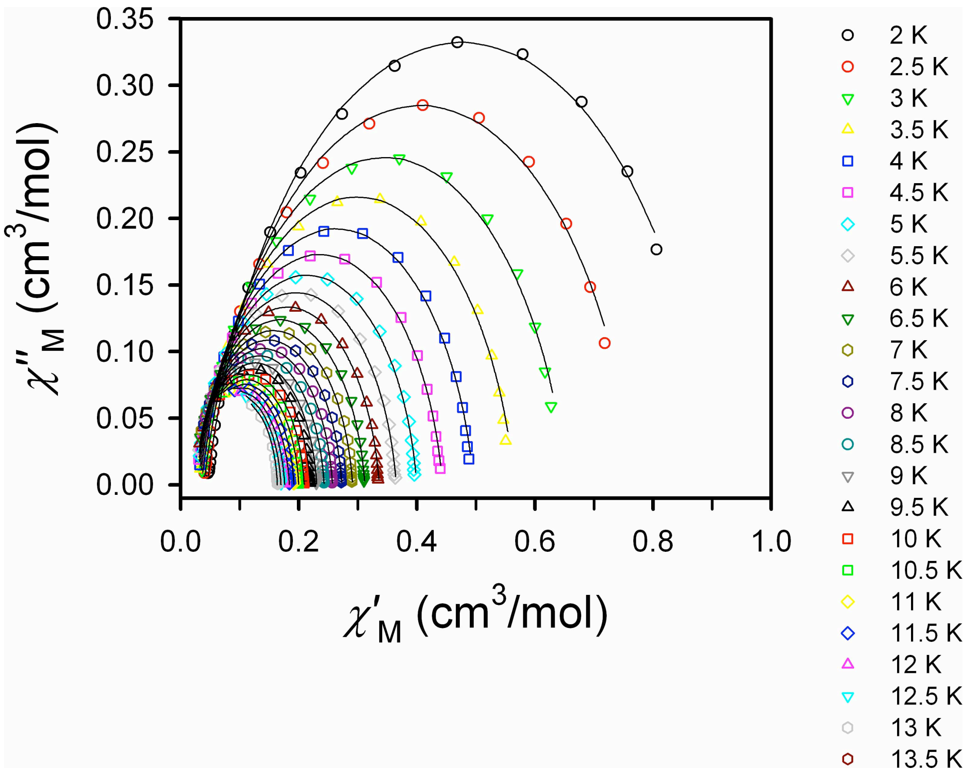

Figure S23. Cole-cole plots of the frequency dependence of χ_M' and χ_M'' used to evaluate the temperature dependence of τ for **4**. Black lines are fits to the general debye model as described in the main text.

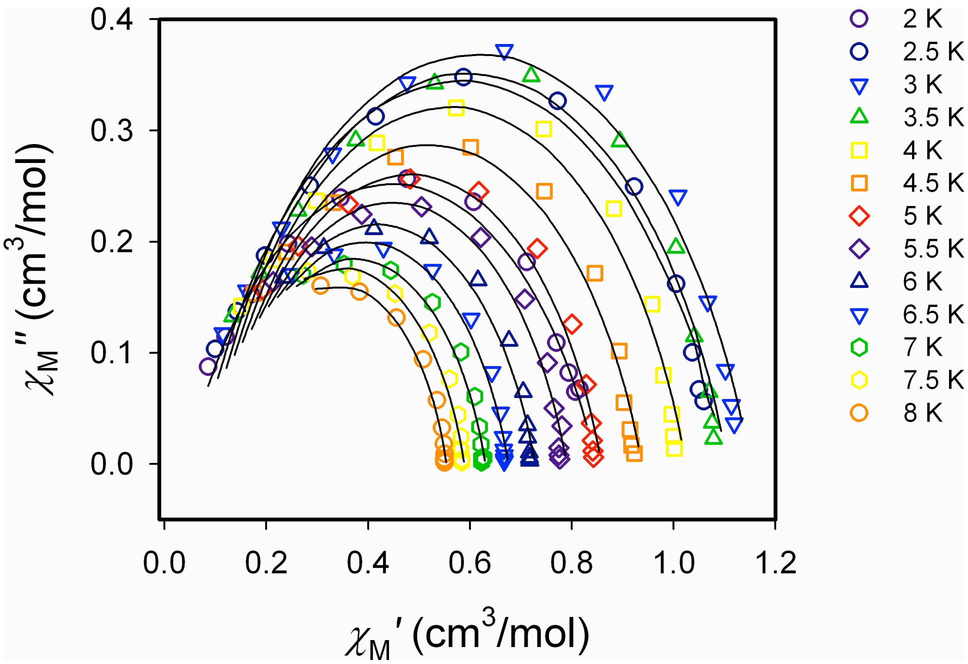

Figure S24. Cole-cole plots of the frequency dependence of χ_M' and χ_M'' used to evaluate the temperature dependence of τ for **5**. Black lines are fits to the general debye model as described in the main text.